Universidad Autónoma de San Luis Potosí.

Facultad de Ciencias

Crystallization of a quasi-two-dimensional granular dimer gas

TESIS

Que para obtener el Grado de

Maestro en Ciencias

P R E S E N T A :

Juan Luis Aguilera Servín

ASESOR:

Dr. Yuri Nahmad Molinari

SAN LUIS POTOSÍ, S.L.P. SEPTIEMBRE 2008

Abstract

We experimentally investigate the crystallization of a uniformly vibrated quasi-2D granular dimer gas (Γ = 6) as a function of the filling fraction. We study the angle dependent radial distribution function and by introducing a relative angle distribution, our results show that for a quasi-2D granular dimer gas there is no translation of the location of ϕ_t(critical filling fraction) when a monomer system is constrained to dimers.

The most exciting phrase to hear in science, the one that heralds new discoveries, is not "Eureka!", but "That's funny..."

Isaac Asimov

Acknowledgements

I would like to thank my supervisor PhD Yuri Nahmad Molinari for directing this thesis.

I express my gratitude to Andrés García Castillo for his idea on studying a 2D granular dimer gas in analogy to the one studied by him in colloids, to María de los Angeles Ramírez Saito and the Complex Fluid Laboratory for part of the software used in this thesis.

I thank PhD Jesús Urias Hermosillo and PhD Juan Faustino Aguilera Granja for the valuable discussion regarding the angle difference analysis.

I am grateful for all the help given by my girlfriend Irma during my whole research.

I thank my family, especially Papá, Mamá, Marcos, Karina, Mamá Anita, Tío Luis and Papá Luis for all their unconditional support through the years.

And finally to CONACYT for the scholarship that allowed me to complete my Master's Degree.

Contents

Chapter 1

Introduction

1.1 Granular matter

The physics of granular materials deals primarily with macroscopic objects. The term "macroscopic" means here that the objects making up such materials must at the very least be visible for the naked eye [1].

Granular materials display a variety of behaviors that are in many ways different from those of other substances. They cannot be classified as either solids or liquids. Recently, the unusual behavior of granular systems has led to a number of theories and to a new era of experimentation on granular systems [2].

1.2 Economic Implications and Industrial Problems

Granular materials occupy a prominent place in our culture. The worlwide annual production of grains and aggregates of various kinds is gigantic, reaching approximately ten billion metric tons. Coal accounts for about 3.5 billion tons of total, cements and ordinary construction materials for one billion tons, to which we can add equal amounts of sand and gravel. The processing of granular media and agregates consumes roughly 10 percent of the total en-

ergy produced by men on this planet. As it turns out, this class of materials ranks second, immediately behind water, on the scales of priorities of human activity. As such any advance in understanding the physics of granulars is bound to have a major economical impact.

The industrial technology used in the treatment of granular materials involves a number of processes. First comes the extraction of ores, sands, and gravel, which often relies on dredging. Next comes crushing and grinding, followed by separation. Since raw materials often account for more than 85 percent of the total cost, it is easy to understand why so little effort has been expended to improve the basic technology which often dates back to the nineteenth century. Not much has been optimized, despite the fact of methods of transport (fluidized beds, conveyor beds), storage (silos), and mixing (e.g.,cement trucks) figure in all stages of industrial processing of aggregates. Problems have received primitive solutions at best. The more specialized and developed arena of high-value-added materials include the cosmetic and pharmaceutical industries, specialized chemistry and the food industry, which demands increasingly sophisticated processing technologies [1].

1.3 Objective

In this work our aim is to find the filling fraction[1] for which a quasi-2D granular dimer gas crystallizes by experimentally studying a uniformly vibrated granular gas of dimers using high speed photography.

1.4 Previous Work

The crystallization of two a dimensional granular fluid was studied by Reis et al. [3] using an experimental apparatus adapted from a geometry introduced by Olafsen and Urbach [4]. Their experimental apparatus consisted of a quasi-two-dimensional granular fluid of stainless steel spheres that is uniformly "heated" using sinusoidal vertical vibration with a frequency $f = 50Hz$

[1] This filling fraction is defined as the ratio of the area occupied by the dimers and the total enclosed area in which the dimers are distributed.

and dimensionless acceleration[2] $\Gamma = 4$. They analized the fluid-to-crystal transition, as a function of the filling fraction studying the radial distribution function and the Lindemann ratio γ_m.

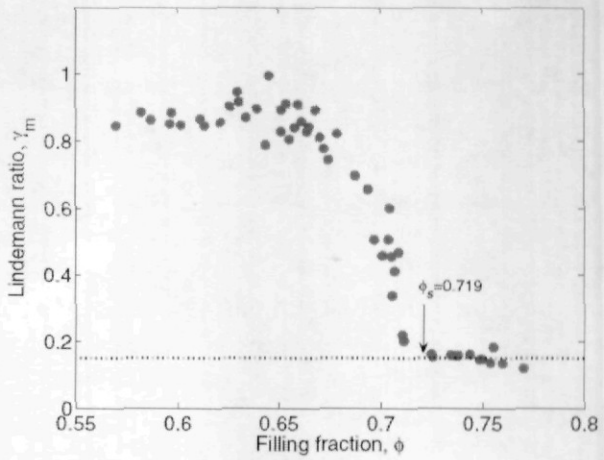

(a)

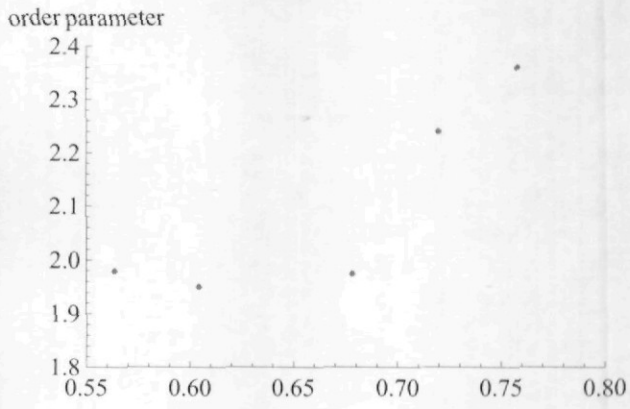

(b)

Figure 1.1: (a) Fluid-to-crystal transition studied by Reis et al. [3], showing the critical filling fraction for a monomer gas. (b)Dimer gas-to-crystal transition studied in this thesis.

Also Straßburger et al. [5] had studied experimentally, the dynamics of a

[2] $\Gamma = A(2\pi f)^2/g$, where A is the amplitude of vibration and g is the gravitational acceleration.

cluster consisting of a few thousand steel spheres on a horizontally vibrated plate, they described a transition from randomly arranged and almost independent moving particles to a two-dimensional crystal-like structure when the filling fraction is increased, this transition was quantitatively characterized by an order parameter obtained from the pair distribution function of the spheres.

On this scenario, the question of the effect of excluded volume forces on the critical filling fraction, in the crystallization transition for a granular dimer gas remains open. The purpose of this work is to determine experimentally, such a effect in the critical filling fraction.

In the field of colloids there was a project which is related to this thesis in which the static structure of quasi-two-dimensional colloidal mixtures of dumbbells and spheres was studied by Andrés García-Castillo and J.L. Arauz-Lara [6], using optical microscopy. . The static structural properties of that system are determined for various concentrations of spheres in the dilute limit of dumbbells. The dumbbell-sphere pair correlation function exhibits a strong angular dependence, and also shows that the presence of dumbbells favors the formation of triangular lattices even at sphere concentrations far from close packing.

The experimental dynamics of a granular dimer gas has not been studied, however a numerical approach has been reported by Costantini et al. [7], where they studied a two-dimensional gas of inelastic smooth hard dimers by deriving an algorithm to study the decay of the total kinetic energy, and of the ratio between the rotational and the translational kinetic energy of inelastic dimers.

Chapter 2

Experimental setup and methods

In our study, we have developed an experimental system to generate a vibrated quasi-two-dimensional granular dimer gas; the experimental apparatus consists of an acrylic cell that is mounted horizontally on a speaker. The cell is composed by two plates of 29.5 cm in diameter which are separated by 0.37 cm height slabs (1.2 Diameters[1]), the bottom plate is roughened[2]. This roughness was produced by manually engraving a random shape pattern using a hot metallic tip. Inside the cell there is a plastic band which restraints within a circle the movement of the particles. The type of particles used for the experiments were dimers made of carbon steel spheres (precision ball bearings) with a diameter of 3.175 mm, the dimers were glued using cyano-acrylat based glue.

As the system is nearly 2D, a camera placed above the cell can capture the horizontal dynamics of any particle in the system[3] (Fig.2.1). By carefully leveling the system, the camera and the cell are located in parallel planes. The particles are illuminated by three light bulbs that are placed perpendicular to the cell, they are positioned in order to achieve a single bright spot on the top of the spheres, this illumination enables an accurate determination of the location of the particles' center location. All experiments were performed using a frequency of 55 Hz; this particular value produces neither resonances,

[1] refering to the particle diameter

[2] The purpose of the roughness is to endow to the particles with horizontal motion.

[3] We track the particle trajectories in a $(53 \times 43)\text{mm}^2$

nor nodes in the system that could lead to an inhomogeneous distribution of particles in the cell.

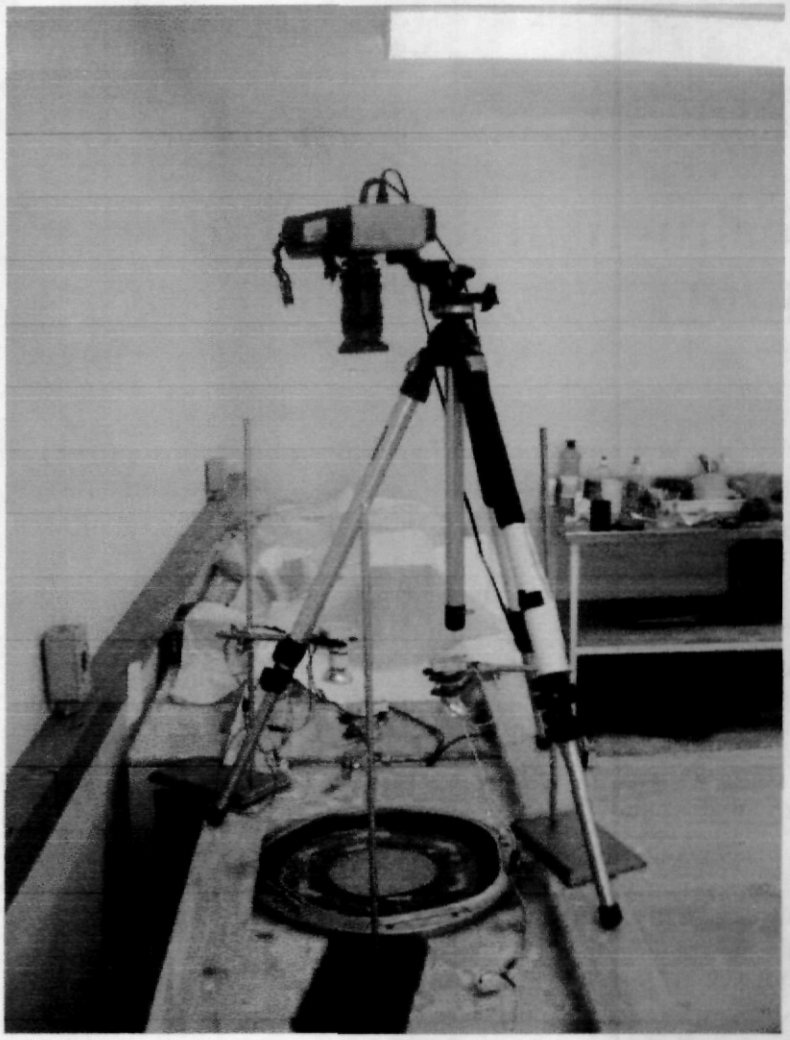

Figure 2.1: Experimental set up in which the camera is placed above the vibrational system.

2.1 Experimental equipment

The video camera used is a Red Lake Motion Meter that records a video event in an internal digital memory, and it's able to replay the event at playback speeds from 1 frame per second (fps) to 1000 fps. The Camera provides a composite NTSC or PAL video output signal. Its recording rates are (50 PAL, 60 NTSC), 125, 250, 500, and 1000 fps.The speaker is 38 cm enclosure type subwoofer (SONY XS-L151P5) with a frequency response of 15 to 2000 Hz. The Function generator is an FG-8002's EZ. All experiments were performed with a fixed sinusoidal wave with a frequency of 55 Hz.

2.2 Experimental method

Our experiment consisted of recording several videos of the dimers for each chosen filling fraction. At each series of experiments, a search (with naked-eye examination) for broken dimers was performed in order to avoid recording an experiment with a broken dimer, whenever a broken dimer was detected, it was replaced with a new one, maintaining the selected filling fraction. The method of recording a series of experiments consists of the following steps: after turning on the wave generator the system of vibrating dimers was left to reach a point of stabilization, for this purpose a time of 45 s was chosen, afterwards the camera was turned on. Just after the camera recorded the experiment, the wave generator was turned off, with the solely purpose of extending the life time of the dimers. The video stored in the internal memory of the camera is playedbacked to a speed of 30 fps and subsequently recorded on a DVD for data analysis. The camera stored the video in an internal memory, in order to be able to analyze the data, this stored information is playbacked to a speed of 30 fps and subsequently recorded in a DVD by connecting the camera to a DVD recorder, once more the wave generator was turned on, the system was left to stabilize and so forth.

Chapter 3

Data Analysis

Upon completing the recording stage, the frames of the video were extracted using commercial software[1]. Each individual frame was analyzed using an ex professo software[2] that was developed using IDL programming language, which extracts the coordinates of the particles' center. Having the coordinates of the particles it was possible to identify the pair of particles which corresponded to a single dimer by comparing the average distance between the trajectories of all pairs of particles, those corresponding to an average distance of one diameter are the particles which correspond to a particular dimer.

For the analysis of the results, the center of each dimer is determined just by computing the coordinates of the particles center (x_1, y_1), (x_2, y_2) that form each dimer. The $(0, 0)$ point of reference corresponds to the bottom right corner of the frame.

An angle for each dimer is assigned, using the slope of the straight line that passes trough (x_1, y_1) and (x_2, y_2) (Fig.3.1).

3.1 Relative angle distribution

Consider the set of angles $X_1 = \{\theta_1, \theta_2, ..., \theta_n\}$, with the angle θ_i corresponding to the i-esim dimer at a particular time, next calculate the difference between all pairs of angles in the set, obtaining in this way a new set

[1]CLONEDVD2, DGIndex, GordianKnot, OSS Video Decompiler.

[2]Provided by the IF-UASLP Complex Fluids Laboratory.

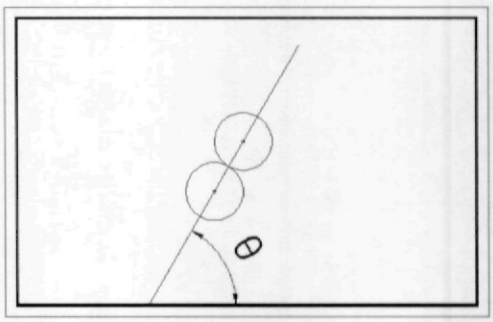

Figure 3.1: Angle that subtends the dimer with the bottom line.

$X_2 = \{\Delta\theta_1, \Delta\theta_2, ..., \Delta\theta_{n\times n}\}$. With the former set, we can create a plot of the distribution of $\Delta\theta$, at this point an immediate question arises: What does the distribution of $\Delta\theta$ look like for a set of θ that follows a rectangular distribution? to answer this, take a look in the following example.

3.1.1 5×5 case

First we introduce a schematic representation of the cartesian product of the set X_1 with itself (Table3.1). A pair of elements (a, b) are located in the box_{ij} if $a \in S_i$ and $b \in S_j$, with $S_k = \left\{d : d \in [(k-1)\frac{180}{5}, k\frac{180}{5}]\right\}$.

11	12	13	14	15
21	22	23	24	25
31	32	33	34	35
41	42	43	44	45
51	52	53	54	55

Table 3.1: Schematic representation of the cartesian product of X_1.

The different pair of elements in the boxes undergo a transformation φ by means of the subtraction of the pair of elements, being the image of this transformation the $\Delta\theta$ distribution. Notice that all the pairs of elements in

the same box under this transformation φ will be located in the same interval. Moreover, elements of the boxes located in the same diagonal will fall under the same interval (Table 3.2).
Now explicitly, we calculate for the first row, to which interval each marked box goes.

$$
\begin{aligned}
\circ &= \{a \times b : a \in [0,36] \ \wedge \ b \in [144,180]\} \longrightarrow A_1 = \{c : c \in [108,180]\} \\
\blacktriangle &= \{a \times b : a \in [0,36] \ \wedge \ b \in [108,144]\} \longrightarrow A_2 = \{c : c \in [72,144]\} \\
\curlywedge &= \{a \times b : a \in [0,36] \ \wedge \ b \in [72,108]\} \longrightarrow A_3 = \{c : c \in [36,108]\} \\
\bigstar &= \{a \times b : a \in [0,36] \ \wedge \ b \in [72,108]\} \longrightarrow A_4 = \{c : c \in [0,72]\} \\
\hexagram &= \{a \times b : a \in [0,36] \ \wedge \ b \in [72,108]\} \longrightarrow A_5 = \{c : c \in [0,36]\}
\end{aligned}
$$

$\circ$	$\blacktriangle$	$\curlywedge$	$\bigstar$	$\hexagram$
$\blacktriangle$	$\curlywedge$	$\bigstar$	$\hexagram$	$\bigstar$
$\curlywedge$	$\bigstar$	$\hexagram$	$\bigstar$	$\curlywedge$
$\bigstar$	$\hexagram$	$\bigstar$	$\curlywedge$	$\blacktriangle$
$\hexagram$	$\bigstar$	$\curlywedge$	$\blacktriangle$	$\circ$

Table 3.2: Diagonals that correspond under the transformation to the same interval.

Now it is possible to determine the probability that a pair (a,b) is going to a particular set under the transformation φ. For example take the case of the interval [0,36], all the pairs of elements that belong to the $\hexagram$ marked boxes, correspond under the transformation φ, to the desired interval, but also the ones with a $\bigstar$, however, in the later case, half the time the subtraction of the pair of elements resides in [36,72], therefore the probability of S_1 is $(5+\frac{8}{2}) \times \frac{1}{25} = \frac{9}{25}$. Using the method described above, one easily encounters that the probabilities of S_2, S_3, S_4, and S_5 are $\frac{7}{25}, \frac{1}{5}, \frac{3}{25}$ and $\frac{1}{25}$, respectively.

Thus, the probabilistic distribution of $\Delta\theta$ for a set of θ that obeys a rectangular distribution follows a straight line (Fig.3.2).

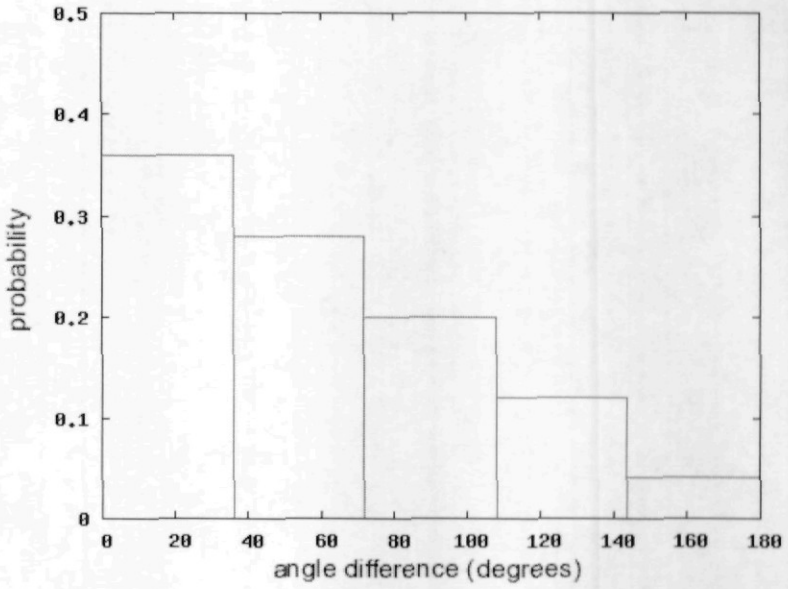

Figure 3.2: Histogram of the probability for the different sets.

3.1.2 $n \times n$ case

In the previous section the 5 × 5 case was developed; in a similar fashion, one can divide the [0,180] interval in three or four subintervals and apply the method described above to obtain the corresponding probabilities, these results are summarized in the table (Table 3.3)

case	1	2	3	4	5
5×5	$9/5^2$	$7/5^2$	$5/5^2$	$3/5^2$	$1/5^2$
4×4	$7/4^2$	$5/4^2$	$3/4^2$	$1/4^2$	-
3×3	$5/3^2$	$3/3^2$	$1/3^2$	-	-

Table 3.3: Different probabilities for the studied cases.

We can conclude that the probability that an angle difference belongs to a particular S_k follows the following formula:

$$\frac{2m-1}{n^2} \qquad m = n, n-1, ..., 1 \quad , \tag{3.1}$$

where n is the number of subintervals in which [0,180] is divided.

A case of interest for our study is the 180×180 (Fig.3.3), since, as shown later, the angle difference distribution for all the studied filling fractions are compared to this ideal distribution.

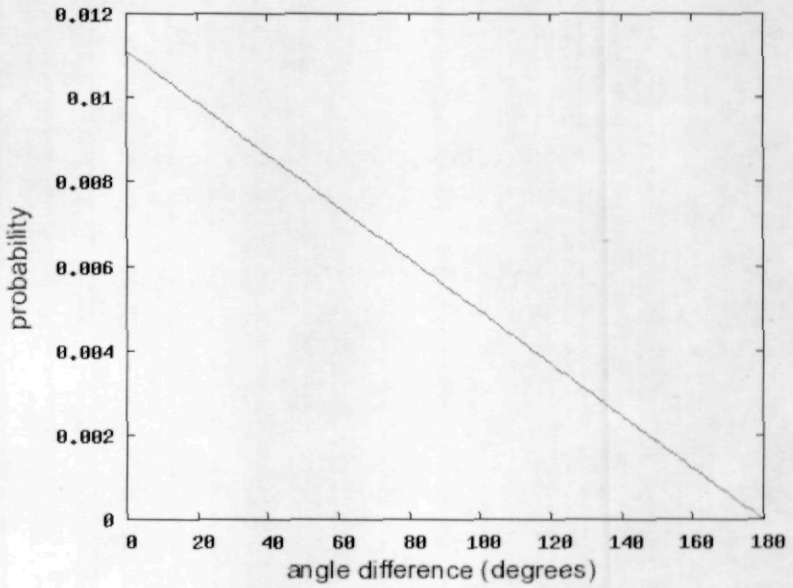

Figure 3.3: Probability function for the 180×180 case.

3.2 Experimental resolution of the angle

Like any measurement that is made in an experiment, the angle θ_i that correspond to the i-esim dimer has an uncertainty $\delta\theta_i$. To give an estimate of $\delta\theta$, consider the uncertainty δx of the coordinates of the center of the particles. Let $(x_1 \pm \delta x, y_1 \pm \delta x)$ and $(x_2 \pm \delta x, y_2 \pm \delta x)$ be the coordinates of the particles

centers that form a particular dimer, then $\delta\theta_i$ can be found via:

$$\delta\theta_i = \arctan\frac{(y_1+\delta y_1)-(y_2-\delta y_2)}{(x_1-\delta x_1)-(x_2+\delta x_2)} - \arctan\frac{y_1-y_2}{x_1-x_2} \quad . \tag{3.2}$$

Equation 3.2 can be readily found considering the maximum change in the slope of the straigh line that passes through the particles' centers, obtaining the corresponding angle and calculating the difference of this angle to the angle calculated using (x_1, y_1), (x_2, y_2).

Equation 3.2 can be further simplified, choosing one particle to be in the point of reference $(0,0)$, that is:

$$\delta\theta_i = \arctan\frac{y_1+\delta y_2+\delta y_1}{x_1-\delta x_1-\delta x_2} - \arctan\frac{y_1}{x_1} \quad . \tag{3.3}$$

Using the fact that in the experiments $\delta z = 0.01z$ (z represents any distance[3]), along with the positions of the particles' centers $(0,0)$ and $(D\cos\theta, D\sin\theta)$, we have that:

$$\delta\theta_i = \arctan 1.04\theta - \arctan\theta \quad , \tag{3.4}$$

where the fact that $\delta y_1 = \delta y_2$ and $\delta x_1 = \delta x_2$ was used.

Therefore the resolution of the angle depends upon the maximum of the equation 3.4, which is approximately $1.1°$ as shown in Fig.3.4.

An example of this limited angle resolution is shown in Fig.3.5 where the angle difference distribution was constructed using the 180×180 case. Here the uncertainty in the angle is a deterministic factor for the central angles $(55-100°)$, leading to a oscillation in the distribution. For $0°$ and $180°$, the relative angle oscillations are due to limited pixel resolution of the camera.

[3]The equivalence of 10 cm in pixels was always measured, and the ruler has an uncertainty of 1 mm

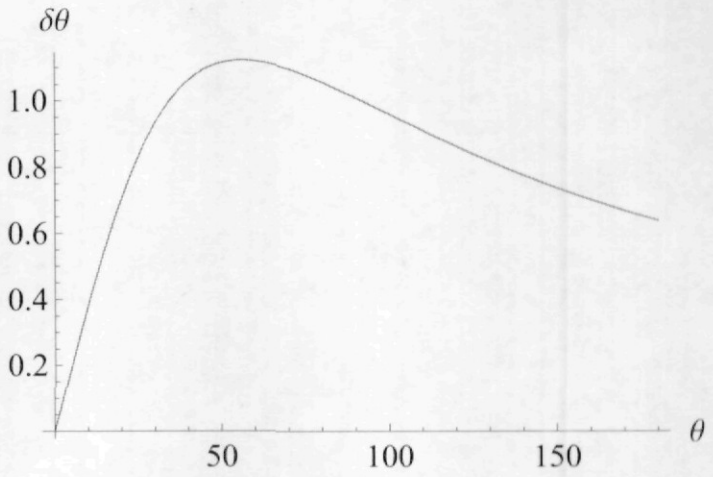

Figure 3.4: Estimated error for a measured angle

3.3 Angular dependence of distance between dimers

Consider two dimers that are in contact, the center of three of its constituents form an equilateral triangle. The distance(d) between the center of the dimers can be obtain in terms of the angle difference θ, to accomplish this, draw a triangle as in Fig.3.6 , since the dimers are in contact $h = D$ where D is the diameter of the particles.

Applying the law of cosines:

$$d^2 = (x + r) + y^2 - 2(x + r)y\cos\theta \quad . \tag{3.5}$$

Using trigonometry, $x = \frac{\sqrt{3}}{2}\cos\theta$, $y = \frac{\sqrt{3}}{2}\cot\theta$, then substituting in 3.5

$$d = \sqrt{1 + \frac{\sqrt{3}}{2}\sin\theta} \quad . \tag{3.6}$$

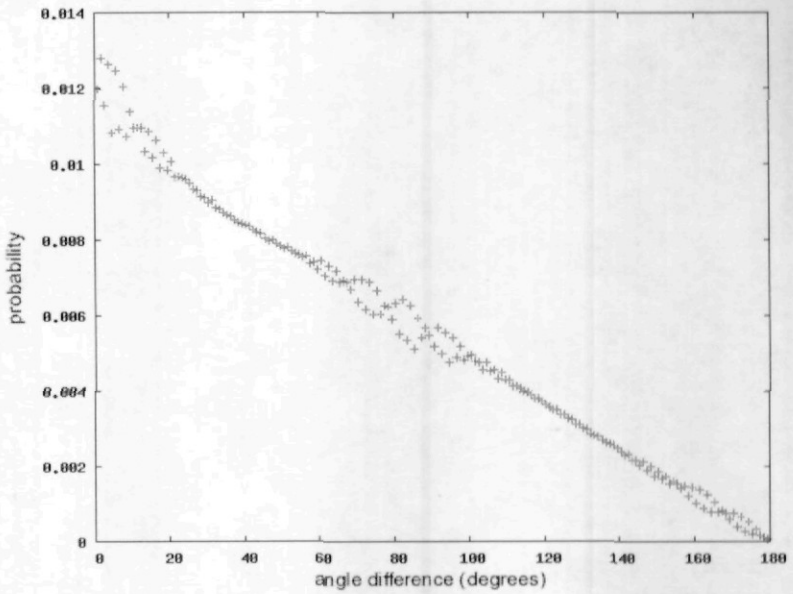

Figure 3.5: In this figure an experimental distribution of relative angles is shown, the oscillation near the relative angles of 0°, 90° and 180° are due to the corresponding low experimental resolution of those angles.

The statistics of the experiments, the angle dependence radial distribution functions has a limited resolution, they will be shown using intervals of 3 degrees, thus the measured distance between dimers will be a result of averaging the distance given by equation in the corresponding interval:

$$\frac{60}{\pi}\int_{\frac{\pi}{60}i}^{\frac{\pi}{60}(i+1)}\sqrt{1+\sqrt{3}/2\sin\theta}\,d\theta \qquad i=0,1,...,29 \quad . \tag{3.7}$$

The numerical values of equation 3.7 were calculated using Mathematica, the results are shown in Fig. 3.7.

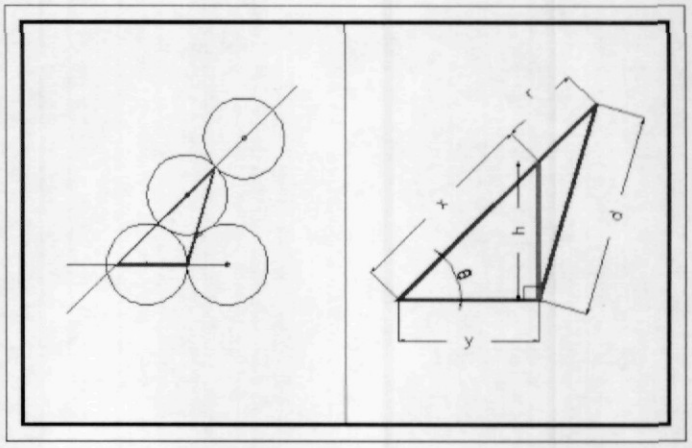

Figure 3.6: Triangle relating d to θ

3.4 Angle dependant radial distribution function

Since the radial distribution function $g(r)$ is defined as the ratio of the probability of finding a particle in a given subvolume dV, at r and the probability of finding a particle in dV if the particles were uniformly distributed [8], an angle dependant radial distribution function $g(r, \Delta\theta)$ is proposed as following:

$$n_{\Delta\theta} = g(r, \Delta\theta) N_{\Delta\theta} \quad , \tag{3.8}$$

where $n_{\Delta\theta}$ is the number of pairs of dimers in $(r, r+\delta r)$ which angle difference is $\Delta\theta$, $N_{\Delta\theta}$ is the number of pairs of dimers in $(0, r+\delta r)$.

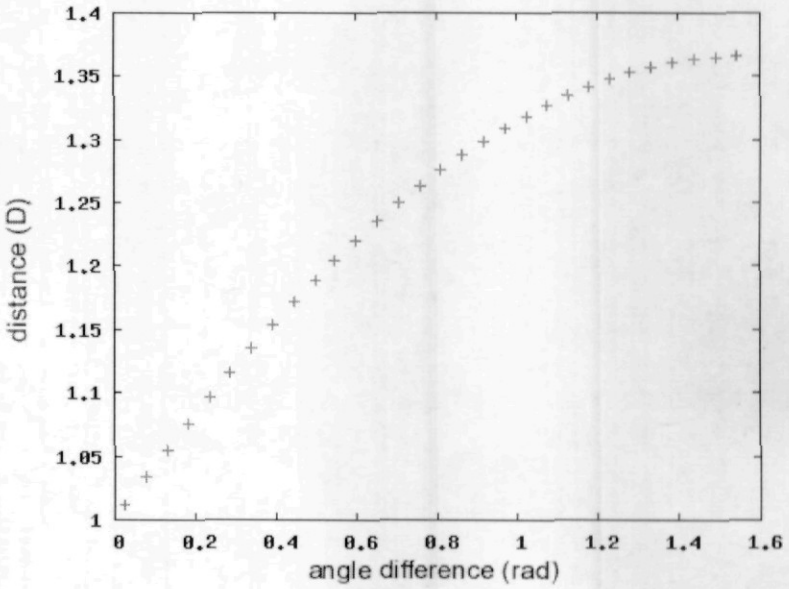

Figure 3.7: numerical results of eq. 3.7.

Chapter 4

Results

As pointed out in the introduction, the main aim was to investigate the crystallization of a dimer gas as a function of the filling fraction. The very first approach was to focus on the angle dependant radial distribution function ($g(r, \Delta\theta)N_{\Delta\theta}$), however a meticulous analysis lead us to discover that within the angle difference distribution was the key factor that enabled us to choose a suitable order parameter which made evident the crystallization.

Eight filling fractions were selected to cover the entire spectrum from high to low packed systems: 0.7583, 0.7198, 0.6785, 0.6045, 0.5637, 0.4822, 0.4058, 0.3465.

In this chapter the angle dependant radial distribution functions are shown for the most representative filling fractions, then we compare the angle dependence of distance between dimers that was found experimentally to the one found theoretically and finally the crystallization graph is presented.

4.1 Angle dependant radial distribution function

The angle dependant radial distribution function $g(r, \Delta\theta)$ is shown in two different views for the 0.3465 (Fig. 4.3 and 4.4), 0.6045 (Fig. 4.5 and 4.6), 0.7198 (Fig. 4.7 and 4.8). According to our analysis there is no substantial change for the $g(r, \Delta\theta)$ from 0.35 to 0.6045, these $g(r, \Delta\theta)$ are characterized

by a noisy structure. At 0.6045 a definite structure starts to arise as seen in (Fig. 4.5). The highest packing experiments that we performed are for 0.7198 and 0.7283 filling fractions, in these an hexagonal-close-packed-like is the ubiquitous structure. The limit for the experiment is when we are no longer able to identify a unique pair for each particle composing a dimer[1], actually at 0.7583 this double assigment is present when false-distances less than one diameter appeared. By analazing the highest points in $g(r, \Delta\theta)$ for each $\delta\theta$ in the 0.7198 filling fractions, it is shown in Fig.4.1 that definite maximus appeared in [0,3] and [60,63] degrees, these relative angles are characteristic of an hexagonal-close-packed(hcp) structure.

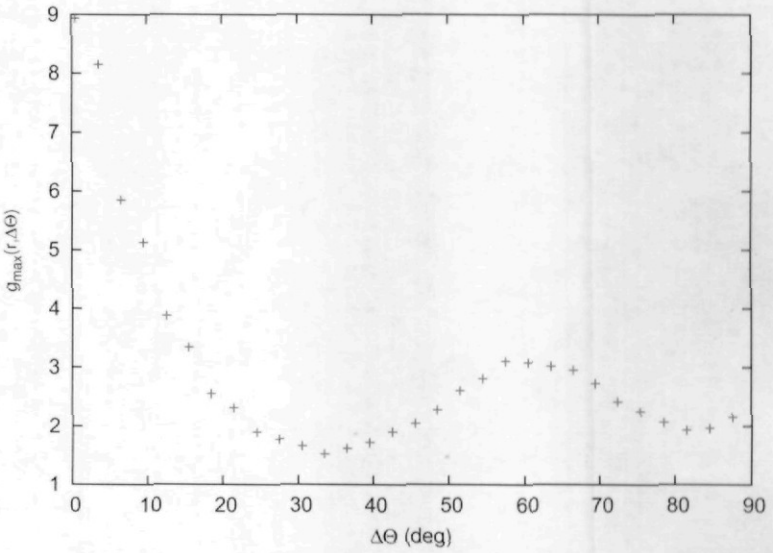

Figure 4.1: Cross section for $g(r, \Delta\theta)$ for $\phi = 0.7198$.

[1] A 2D hexagonal-close-packed structure posses a filling fraction of 0.917, the closer one gets to this number the harder is to identify the pairs of particles for each dimer.

4.2 Experimental angular dependence of distance between dimers

At this point we compare the theorical and experimental distances between dimers. Fig. 4.2 was constructed using the values of r in $g(r, \Delta\theta)$ for which there is a maximum for each $\Delta\theta$. The discrepance at the high filling fraction could be due to the restriction of larger angle differences in an hexagonal-close-packed like structure, that is, since the most common first neighbor relative angles in an hcp structure are 0 and 60 degrees.

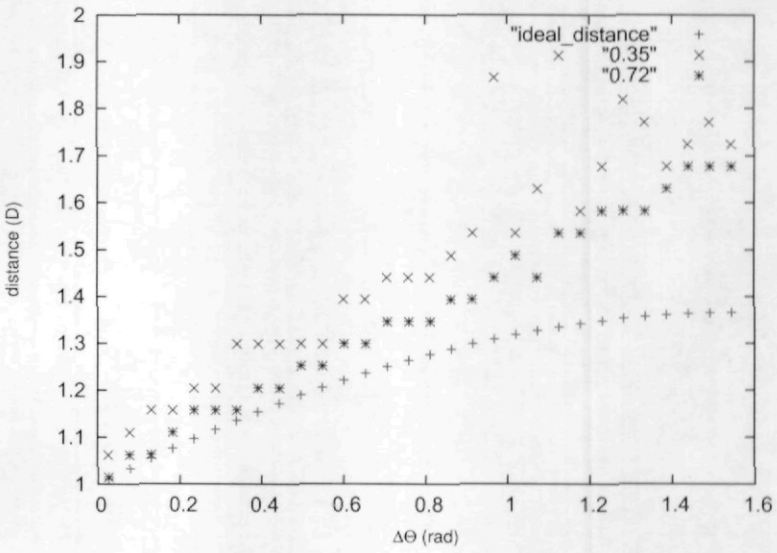

Figure 4.2: Comparison between theorical and experimental distances between dimers.

4.3 Crystallization of a quasi-two-dimensional granular dimer gas

Since we know the form of the random angle difference distribution, and for each selected filling fraction we have a particular angle difference distribution, we can compare each one of them by dividing the random distribution and

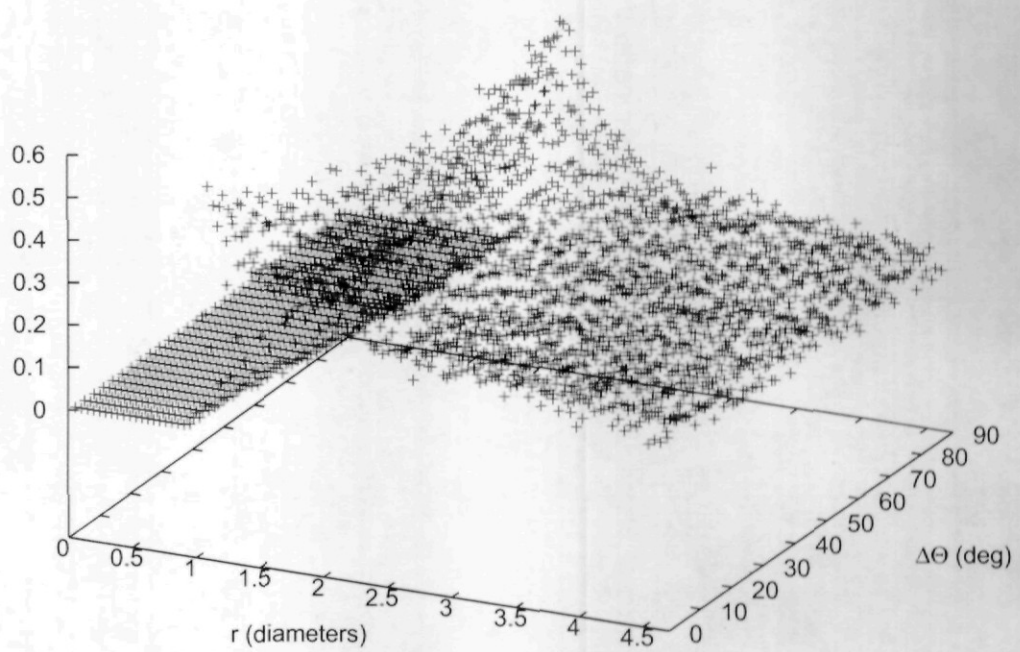

Figure 4.3: $g(r, \Delta\theta)$ for a filling fraction of 0.3465.

the angle difference (Fig. 4.9), this plot gives us a clue about which should be the selected order parameter, notice that the most packed filling fractions peaked at 120 and 60, thus we defined the order parameter as the sum of the relative probabilities of 120 and 60 degrees for each filling fraction. This parameter clearly shows that a transition occurs in $\phi_t = 0.7198$ (Fig. 4.11).

A really interesting result is that we found that the transition occurs at the same filling fraction reported by Reis et al. [3], recall as shown in Fig. 1.1 that their reported filling fraction is 0.719, just the same as ours even

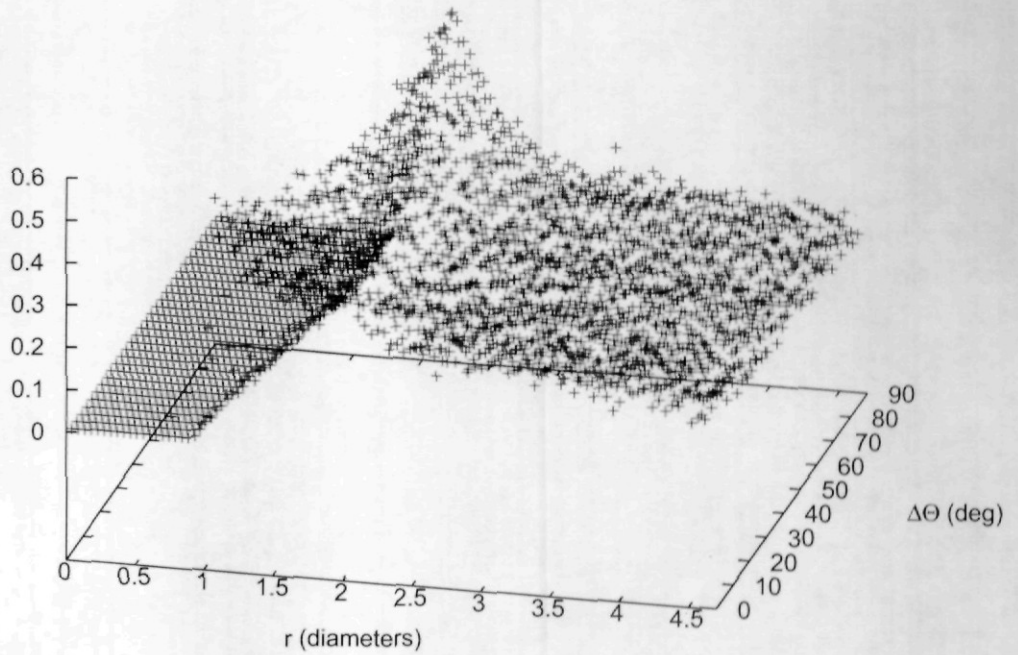

Figure 4.4: $g(r, \Delta\theta)$ for a filling fraction of 0.3465.

though we studied dimers. This result surprising at first, is not that strange, if we consider the fact that in order to form a hexagon with dimers at least we need 4 (Fig.4.10), in this case each possible hexagonal structure posses an extra particle that at not packed filling fractions induces spacing, therefore breaking the formation of larger hexagonal-like clusters. This situation will not happen when we choose a combination of dimers and trimers for instance where a perfect hexagon is possible and readily accessible to low packed systems. This results shows that at least for granular matter there is no translation of the location of ϕ_t when a monomer system is constrained to dimers.

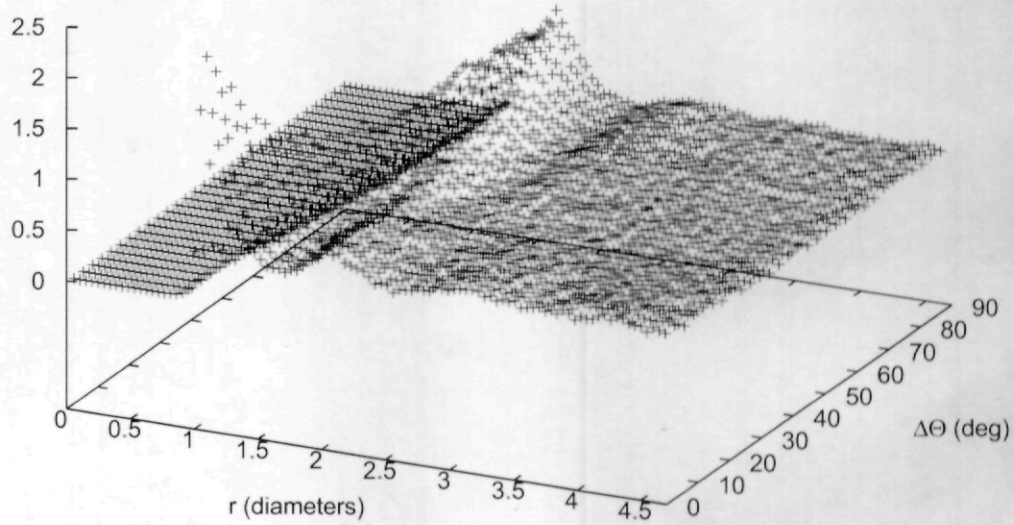

Figure 4.5: $g(r, \Delta\theta)$ for a filling fraction of 0.6045.

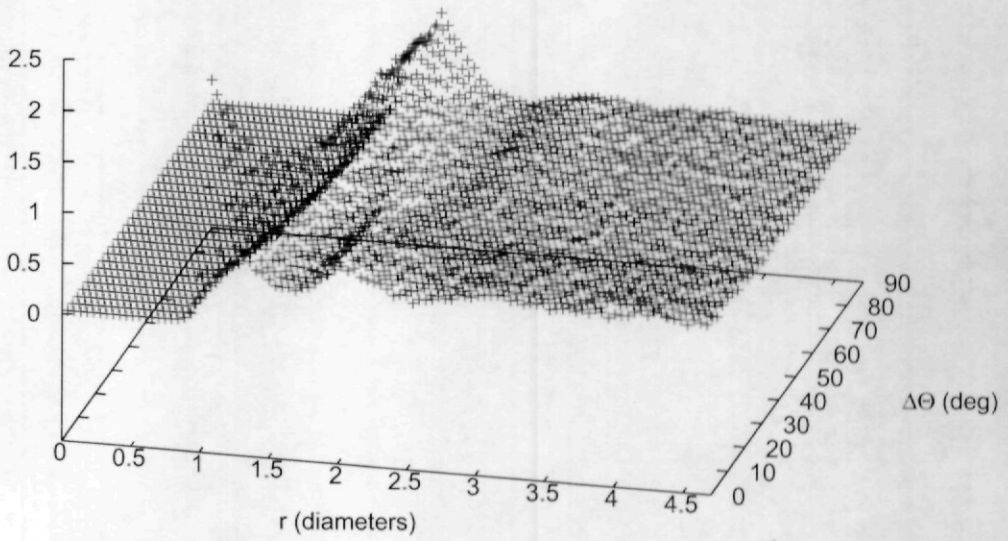

Figure 4.6: $g(r, \Delta\theta)$ for a filling fraction of 0.6045.

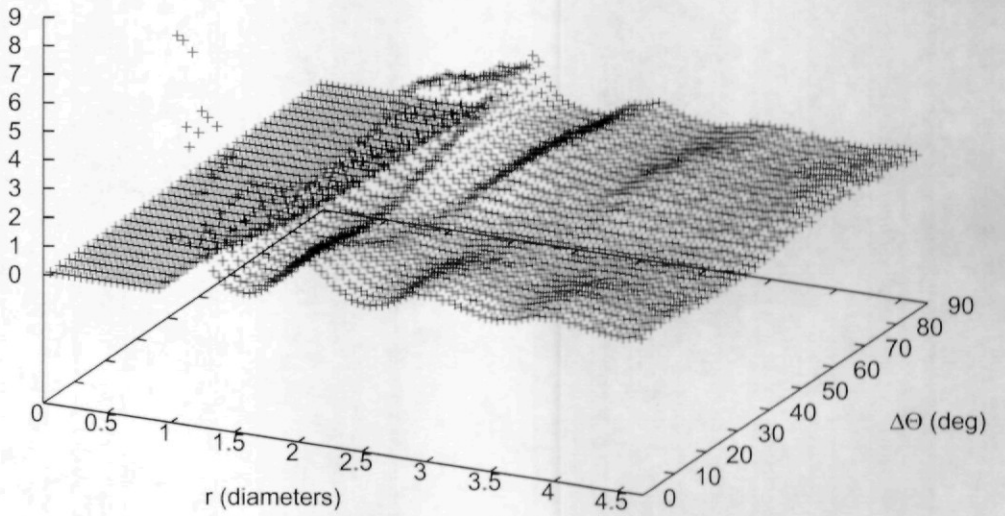

Figure 4.7: $g(r, \Delta\theta)$ for a filling fraction of 0.7198.

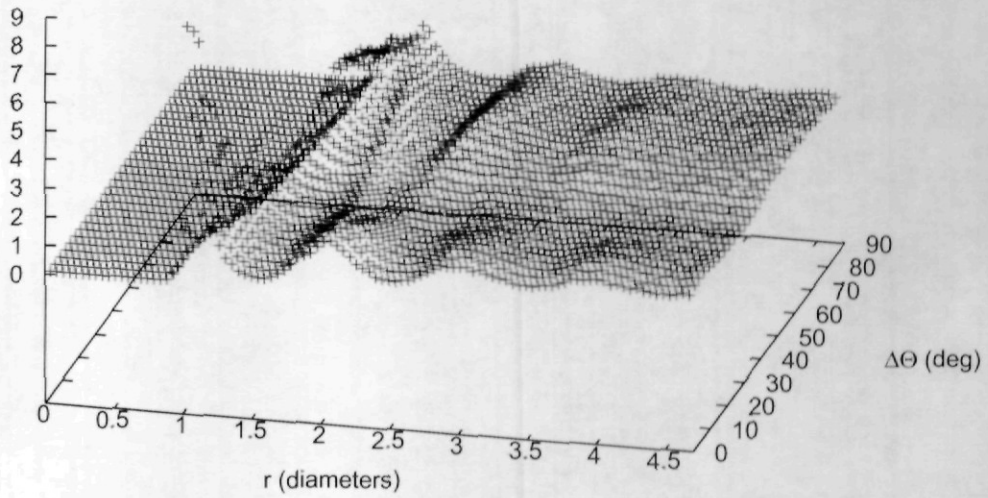

Figure 4.8: $g(r, \Delta\theta)$ for a filling fraction of 0.7198.

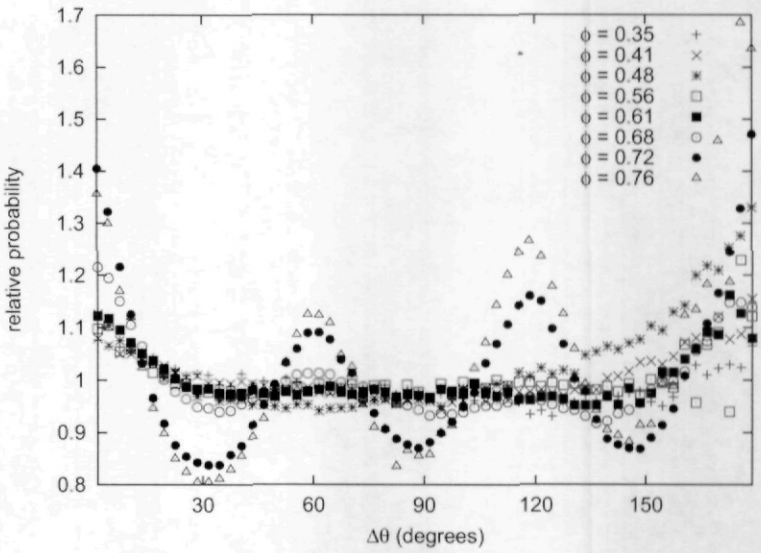

Figure 4.9: Relative probability for several filling fractions

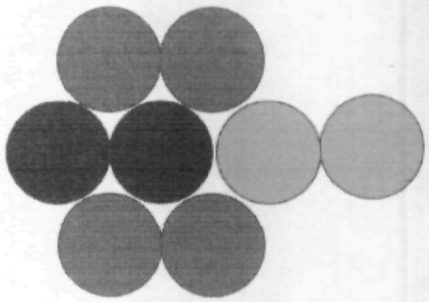

Figure 4.10: Hexagon formed by 4 dimers.

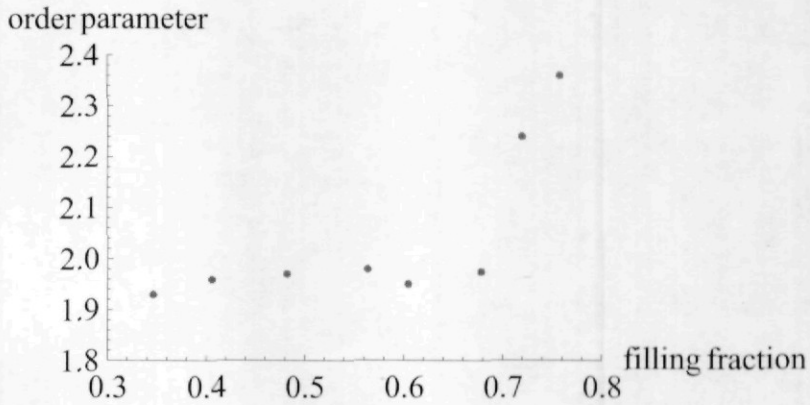

Figure 4.11: Fluid-to-crystal transition in a granular dimer gas

Chapter 5

Summary and Conclusions

We created an experiment for studying a quasi-2D granular dimer gas, we performed a relative angle difference analysis and we obtained angle dependant radial distribution functions for the 0.7583, 0.7198, 0.6785, 0.6045, 0.5637, 0.4822, 0.4058, 0.3465 filling fractions.

We showed that for a quasi-2D granular dimer gas there is no translation of the location of ϕ_t(critical filling fraction) when a monomer system is constrained to dimers.

5.1 Conclusions

We conclude that the probability that a relative angle belongs to a particular S_k follows the following formula:

$$\frac{2m-1}{n^2} \qquad m = n, n-1, ..., 1 \tag{5.1}$$

where n is the number of subintervals in which [0,180] is divided.

A uniformaly vibrated ($\Gamma = 6$) quasi-2D granular dimer gas crystallizes when reaches a critical filling fraction of $\phi_t = 0.7198 \pm 0.0001$ [1].

[1] $\Delta\phi_t$ was obtained by calculating the standard error of the mean

5.2 Future Work

As mentioned earlier, the limitation for our experiment is when we are no longer able to identify a pair of particles for each dimer for large filling fractions, thus a defiant problem is to improve the software used in this thesis and with that extend the experimental points in Fig.4.11 as closest to 0.917 as possible.

An extensive analysis on the angle dependant radial distribution functions obtained, must be performed in order to identify a corresponding microstructure for each filling fraction.

With this work, we have established the bases for studying quasi-2D granular dimer gas, the experimental set-up will be useful for researching on combinations of monomers, dimers, trimers and so on.

Appendix A

System homogeneity

To measure the homogeneity of our vibrational system (Speaker + Cell), we divide the area of a photo in 12 subareas, we calculate the normal density of particles in each area for a sample of 16000 frames ($\phi = 0.4822$) and finally we compare that density to the density of an ideal homogeneous system in which each area posses a normal density of $1/12$. Our results are summarized in Table A.1, where it is shown that there is a uniform distribution of particles in all areas but the one located in the right upper corner, this variation must be due to the inherent improvised nature of such a experimental system.

1.01	1.00	1.03	1.15
0.98	1.02	0.96	1.01
0.95	0.95	0.98	0.96

Table A.1: Average normal density of particles for the Speaker + Cell system.

Bibliography

[1] Jacques Duran. *Sands, Powders and Grains.* Springer, 1997.

[2] H. M. Jaeger and Sidney R. Nagel. Physics of the Granular State. *Science*, 255(5051):1523–1531, 1992.

[3] P. M. Reis, R. A. Ingale, and M. D. Shattuck. Crystallization of a quasi-two-dimensional granular fluid. *Physical Review Letters*, 96(25):258001, 2006.

[4] J. S. Olafsen and J. S. Urbach. Velocity distributions and density fluctuations in a granular gas. *Phys. Rev. E*, 60(3):R2468–R2471, Sep 1999.

[5] G. Straßburger and I. Rehberg. Crystallization in a horizontally vibrated monolayer of spheres. *Phys. Rev. E*, 62(2):2517–2520, Aug 2000.

[6] Andres Garcia-Castillo and Jose Luis Arauz-Lara. Static structure of confined dumbbell-sphere colloidal mixtures. *Physical Review E (Statistical, Nonlinear, and Soft Matter Physics)*, 78(2):020401, 2008.

[7] Giulio Costantini, Umberto Marini Bettolo Marconi, Galina Kalibaeva, and Giovanni Ciccotti. The inelastic hard dimer gas: A nonspherical model for granular matter. *The Journal of Chemical Physics*, 122(16):164505, 2005.

[8] K. Younge, C. Christenson, A. Bohara, J. Crnkovic, and P. Saulnier. A model system for examining the radial distribution function. *American Journal of Physics*, 72(9):1247–1250, 2004.